



Acute silencing of hippocampal CA3 reveals a dominant role in place field responses

Heydar Davoudi ^{1,2,3,4} and David J. Foster ^{1,2,3*}

Neurons in hippocampal output area CA1 are thought to exhibit redundancy across cortical and hippocampal inputs. Here we show instead that acute silencing of CA3 terminals drastically reduces place field responses for many CA1 neurons, while a smaller number are unaffected or have increased responses. These results imply that CA3 is the predominant driver of CA1 place cells under normal conditions, while also revealing heterogeneity in input dominance across cells.

The hippocampus plays a critical role in memory, and two systems-level mechanisms are thought to support this role: the spatially localized responses of individual hippocampal neurons during locomotion, and the coordinated activity of large numbers of neurons during rest reflected in the local field potential (LFP) as high frequency (100–250 Hz) sharp-wave-ripple (SWR) events¹. The output area of the hippocampus, CA1, receives multiple excitatory inputs, including from entorhinal cortex and hippocampal CA3 and CA2, and numerous previous studies have suggested that redundancy governs their role in driving both place field responses^{2–7} and ripple-related activity^{5,7–9}. Early studies suppressing CA3 reported only minimal changes to CA1 place responses^{2,3}. A recent molecular genetic approach, blocking vesicle release at CA3 terminals, caused increased CA1 place field sizes, while peak firing rates were unaffected⁴, as was ripple incidence in the LFP⁵. However, the suppression of CA3 output was always prolonged before the measurement of CA1 activity, either due to animal recovery and electrode adjustment following surgery³, or the 6–8 weeks required for genetic expression^{4,5}. Thus, compensatory changes such as homeostatic plasticity¹⁰ might have occluded a more prominent role for CA3 input. We hypothesized that acute silencing of CA3 input would overcome this limitation.

We virally expressed either the light-activated proton pump eArch3.0 or green fluorescent protein (GFP) control in CA3 neurons in experimental (EXP, $N=4$) or control (CON, $N=2$) rats, respectively, using stereotaxic injections targeted specifically to CA3a,b at multiple sites along the septotemporal axis bilaterally (Fig. 1a and Supplementary Fig. 1a). After 4–6 weeks, expression of eArch3.0 in EXP rats was evident in CA3 cell bodies and in Schaffer collaterals in the stratum radiatum and stratum oriens of CA1, but not in the CA1 and CA2 stratum pyramidale (Fig. 1c–f and Supplementary Fig. 1b,c). In particular, while eArch3.0 was expressed in the axons of CA3 neurons passing through the CA2 subfield, colabeling with CA2 cell bodies demonstrated almost no expression of eArch3.0 (Supplementary Fig. 1c). We used independently depth-adjustable optical fibers to illuminate CA3 terminals bilaterally in the stratum radiatum of dorsal CA1, while simultaneously recording from up to 40 independently depth-adjustable tetrodes gradually lowered bilaterally into the stratum pyramidale of dorsal CA1 (Fig. 1b and

Supplementary Fig. 1d,e). To provide assurance that optical fibers were targeted to the stratum radiatum, a ‘piggy-back’ recording tetrode was attached to, and flush with, the bottom of each optical fiber. The incidence rate and amplitude of SWRs on the piggy-back tetrodes matched the rest of the tetrodes, implying that they were at the same depth (Supplementary Fig. 2a,b). Hence, the light output was delivered to stratum radiatum and not to stratum oriens which was above and behind the fibers. We first examined the effect of acute CA3 suppression while rats were at rest in a sleep box (Supplementary Fig. 3a,b). To avoid overestimation of effect size and significance by repetitive counting across successive recording sessions, only one session was selected for each tetrode per animal, from an initial baseline period before light delivery. This selection process yielded a total of 37 and 88 tetrodes in CON and EXP rats, respectively. The incidence of CA1 SWRs was dramatically suppressed in the majority of EXP tetrodes during light-on periods (ON) compared with light-off periods (OFF), while for CON tetrodes incidence was slightly enhanced (Fig. 1g–i and Supplementary Fig. 2c). There was some variability between EXP tetrodes probably due to variation between tetrodes in the amount of light impinging on axonal input; indeed, the degree of SWR modulation for each tetrode correlated with estimated horizontal distance between tetrode and optical fiber tip for EXP tetrodes, but not for CON tetrodes (Fig. 1j). EXP tetrodes also exhibited a decrease in power spectral density in the ripple frequency band (Supplementary Fig. 2d). We also found subtle abnormalities in the expression of SWRs. Notably, the frequency of SWR peak power was decreased in EXP rats during ON periods, which is consistent with previous studies⁵ (Supplementary Fig. 2e–g). There was a subtle rebound effect in light OFF periods revealed by comparing OFF periods with the initial baseline period. Although both EXP and CON tetrodes did not differ in SWR rate between OFF periods and the baseline, a second-order effect was observed in EXP animals only, in which the degree of negative modulation of SWR rate during ON compared with OFF was correlated with the degree of positive modulation of SWR rate during OFF compared with baseline (Supplementary Fig. 2h). Multiunit spiking was also significantly suppressed in EXP tetrodes during the ON condition, while CON tetrodes were unaffected (Supplementary Fig. 2i–k). Similar results were found for awake SWRs, sampled from stopping periods punctuating periods of locomotive behavior (Supplementary Fig. 4). Overall, these findings pinpoint CA3 as critical for the generation of SWRs and rest-state spiking activity in CA1.

We next considered the contribution of CA3 input to CA1 place field responses. Rats were trained in a linear track running task before recording, for 5–7 days, 30–40 laps (there and back) per day. We delivered light during alternate laps on the familiar linear track

¹Department of Psychology, University of California, Berkeley, Berkeley, CA, USA. ²Helen Wills Neuroscience Institute, University of California, Berkeley, Berkeley, CA, USA. ³Solomon H. Snyder Department of Neuroscience, Johns Hopkins University School of Medicine, Baltimore, MD, USA. ⁴Department of Biomedical Engineering, Johns Hopkins University School of Medicine, Baltimore, MD, USA. *e-mail: davidfoster@berkeley.edu

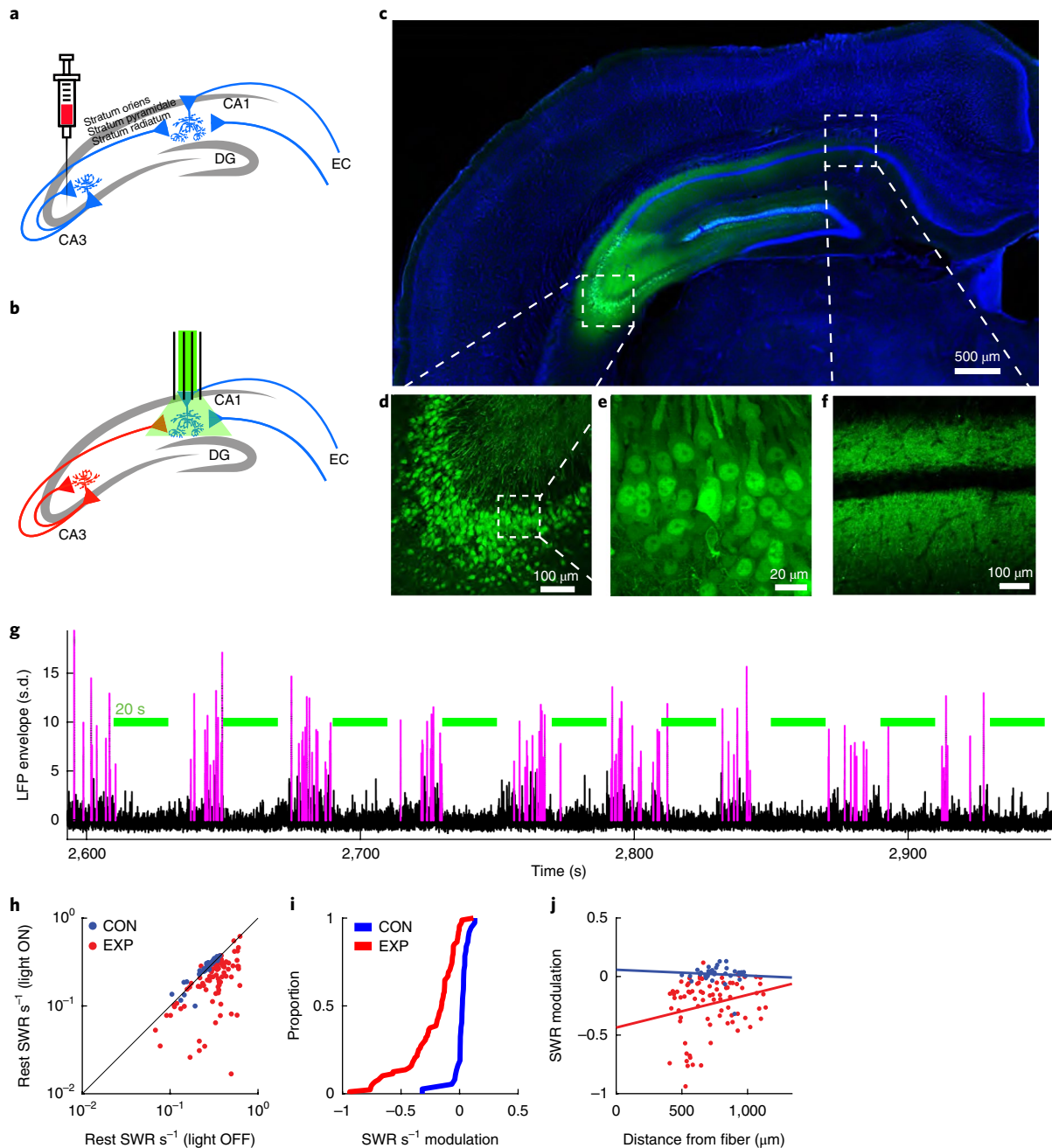


Fig. 1 | CA3 input is necessary for normal SWR activity in CA1. **a,b**, Each rat undergoes two surgeries, the first for virus injection (**a**) and the second for bilateral optrode implantation (**b**). EC, entorhinal cortex; DG, dentate gyrus. **c–f**, An example of expression of virally injected GFP in a coronal slice of rat brain (**c**). In a magnified view, CA3a pyramidal cells strongly express GFP (**d** and **e**) and CA1 pyramidal cells receive CA3 inputs in their stratum radiatum and stratum oriens, below and above the cell layer, respectively (**f**). The blue background signal is from Hoechst 33258 staining. These results were independently repeatable for three more rats as shown in Supplementary Fig. 1b. **g**, An example tetra in CA1 shows strong suppression of SWRs by silencing CA3 input to CA1. Magenta traces are periods in the LFP that meet SWR detection criteria. Green bars denote 20 s light ON periods intermingled with 20 s light OFF periods. **h**, SWR incidence rate for each tetra in light ON versus light OFF conditions. Each dot represents a tetra. CON: OFF: 0.26 ± 0.01 SWR s^{-1} (mean \pm s.e.m.) and ON: 0.27 ± 0.01 , two-tailed signed-rank test, $n = 37$ tetrodes, $z_{(36)} = -3.3$, $P = 0.0008$; EXP: OFF: 0.34 ± 0.01 and ON: 0.22 ± 0.01 , two-tailed signed-rank test, $n = 88$ tetrodes, $z_{(87)} = 7.9$, $P = 5 \times 10^{-15}$. **i**, Cumulative density plot (CDF) of SWR incidence modulation index $([ON - OFF]/[ON + OFF])$ (two-tailed rank-sum test: $n_1 = 37$ and $n_2 = 87$ tetrodes, $z_{(124)} = 7.8$, $P = 10^{-14}$). **j**, The relationship between the horizontal distance of each tetra from optical fiber and the modulation of SWR incidence by light (Pearson's correlation, CON: $r = -0.07$, $n = 37$ tetrodes, two-tailed F statistics, $F_{(36)} = 0.17$, $P = 0.7$; EXP: $r = 0.18$, $n = 82$ tetrodes, two-tailed F statistics, $F_{(81)} = 4.59$, $P = 0.02$).

(Supplementary Fig. 3c). To avoid the possibility of repetitive inclusion of the same place cells from different sessions, we considered only one session for each tetra on the basis of the number of well-isolated clusters. Cell clusters were manually isolated from neural

spike recordings from CON and EXP rats in different run sessions, 220 and 473, respectively, of which 157 and 236 exhibited directional place fields (Fig. 2 and Supplementary Fig. 5). While illumination did not impair expression of place fields in CON place cells, around

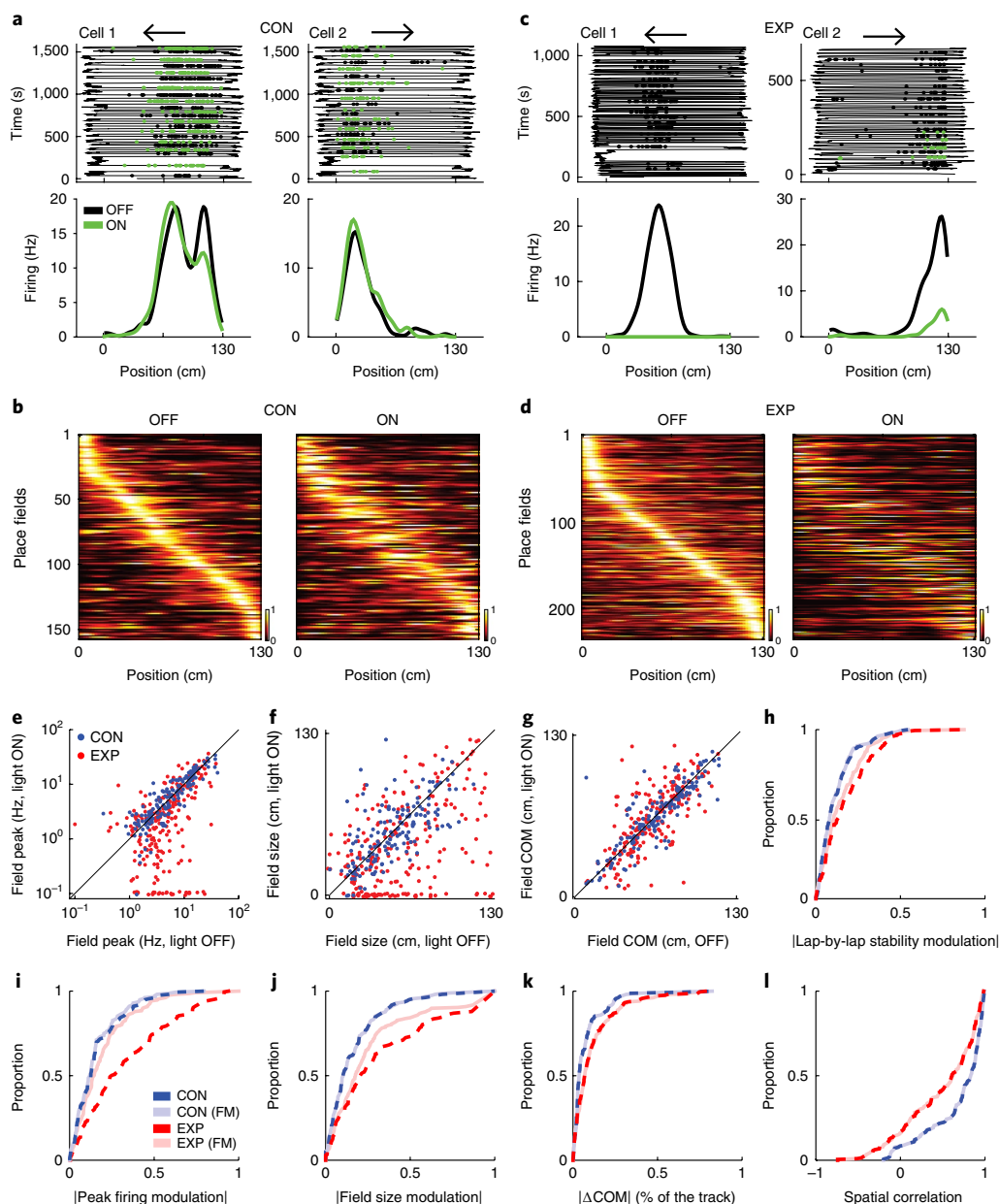


Fig. 2 | CA3 is necessary for normal place field responses in CA1. **a**, Two example CA1 place fields in CON rats. Rat position as a function of time during linear track traversals (thin line), overlaid with spiking activity only in the running direction depicted by the arrow. Top: spikes in light OFF and light ON conditions are shown as black and green dots, respectively. Bottom: the average place fields calculated from above lap-by-lap spiking activities. **b**, All nonrepetitive CON place fields sorted by their peak firing position during light OFF condition on the linear track. Each row depicts the color map of same place field in light OFF (left) and light ON (right) conditions. Each field is normalized by its maximum peak firing rate across OFF and ON conditions and the order of fields is similar between the two light conditions. **c,d**, Two example CA1 place fields (**c**) and all nonrepetitive sorted fields from EXP rats (**d**) as described in **a** and **b**. **e-g**, Place field features in light ON versus light OFF conditions. Values are presented as mean \pm s.e.m. (**e**) Peak firing rate (CON: OFF: 7.97 ± 0.62 Hz and ON: 7.95 ± 0.55 , two-tailed signed-rank test, $n = 157$ fields, $z_{(156)} = -1.1$, $P = 0.3$; EXP: OFF: 6.63 ± 0.43 and ON: 4.70 ± 0.40 , two-tailed signed-rank test, $n = 236$ fields, $z_{(235)} = 5.8$, $P = 10^{-8}$). (**f**) Place field size (CON: OFF: 51.40 ± 1.95 cm and ON: 51.01 ± 1.98 , two-tailed paired t test, $n = 157$ fields, $F_{(156)} = 0.06$, $P = 0.80$; EXP: OFF: 57.58 ± 2.17 and 39.97 ± 2.23 ; two-tailed signed-rank test, $n = 236$ fields, $z_{(235)} = 6.8$, $P = 2 \times 10^{-11}$). (**g**) COM (CON: OFF: 65.81 ± 2.02 cm and 65.81 ± 2.03 , two-tailed paired t test, $n = 156$ fields, $F_{(155)} = 0.00$, $P = 1$; EXP: OFF: 62.89 ± 1.54 and ON: 63.27 ± 1.81 , two-tailed signed-rank test, $n = 207$ fields, $z_{(206)} = -0.1$, $P = 0.9$). **h-l**, the CDF of place field features in CON and EXP rats. (**h**) The CDF of the absolute value of the lap-by-lap stability modulation of original and firing-matched (FM) place fields (original: two-tailed rank-sum test, $n_1 = 156$ and $n_2 = 207$ fields, $z_{(362)} = -3.9$, $P = 2 \times 10^{-4}$; FM: two-tailed rank-sum test, $n_1 = 156$ and $n_2 = 207$ fields, $z_{(362)} = -2.5$, $P = 0.013$; EXP original versus EXP FM: two-tailed signed rank test, $n = 207$ fields, $z_{(206)} = 4.2$, $P = 5 \times 10^{-5}$). (**i**) The CDF of the absolute value of the amount of peak firing rate modulation (original: two-tailed rank-sum test, $n_1 = 156$ and $n_2 = 207$ fields, $z_{(362)} = -6.7$, $P = 3 \times 10^{-11}$; FM: two-tailed rank-sum test, $n_1 = 156$ and $n_2 = 207$ fields, $z_{(362)} = -2.1$, $P = 0.036$). (**j**) The CDF of the absolute value of the amount of field size modulation (original: two-tailed rank-sum test, $n_1 = 156$ and $n_2 = 207$ fields, $z_{(362)} = -5.1$, $P = 5 \times 10^{-7}$; FM: two-tailed rank-sum test, $z_{(362)} = -3.4$, $P = 7 \times 10^{-4}$; EXP original versus EXP FM: two-tailed signed-rank test, $n = 207$ fields, $z_{(206)} = 3.2$, $z_{(362)} = -3.0$, $P = 0.0015$). (**k**) The CDF of the absolute value of the amount of COM shift (original: two-tailed rank-sum test, $n_1 = 156$ and $n_2 = 207$ fields, $z_{(362)} = -3.1$, $P = 0.0025$; FM: two-tailed rank-sum test, $n_1 = 156$ and $n_2 = 207$ fields, $z_{(362)} = -3.3$, $P = 0.001$; EXP original versus EXP FM: two-tailed signed-rank test, $n = 207$ fields, $P = 0.3$). (**l**) The CDF of the spatial correlation (original: two-tailed rank-sum test, $n_1 = 156$ and $n_2 = 207$ fields, $z_{(362)} = 5.0$, $P = 10^{-6}$; EXP original versus EXP FM: two-tailed signed-rank test, $n = 207$ fields, $z_{(206)} = 2.7$, $P = 0.008$).

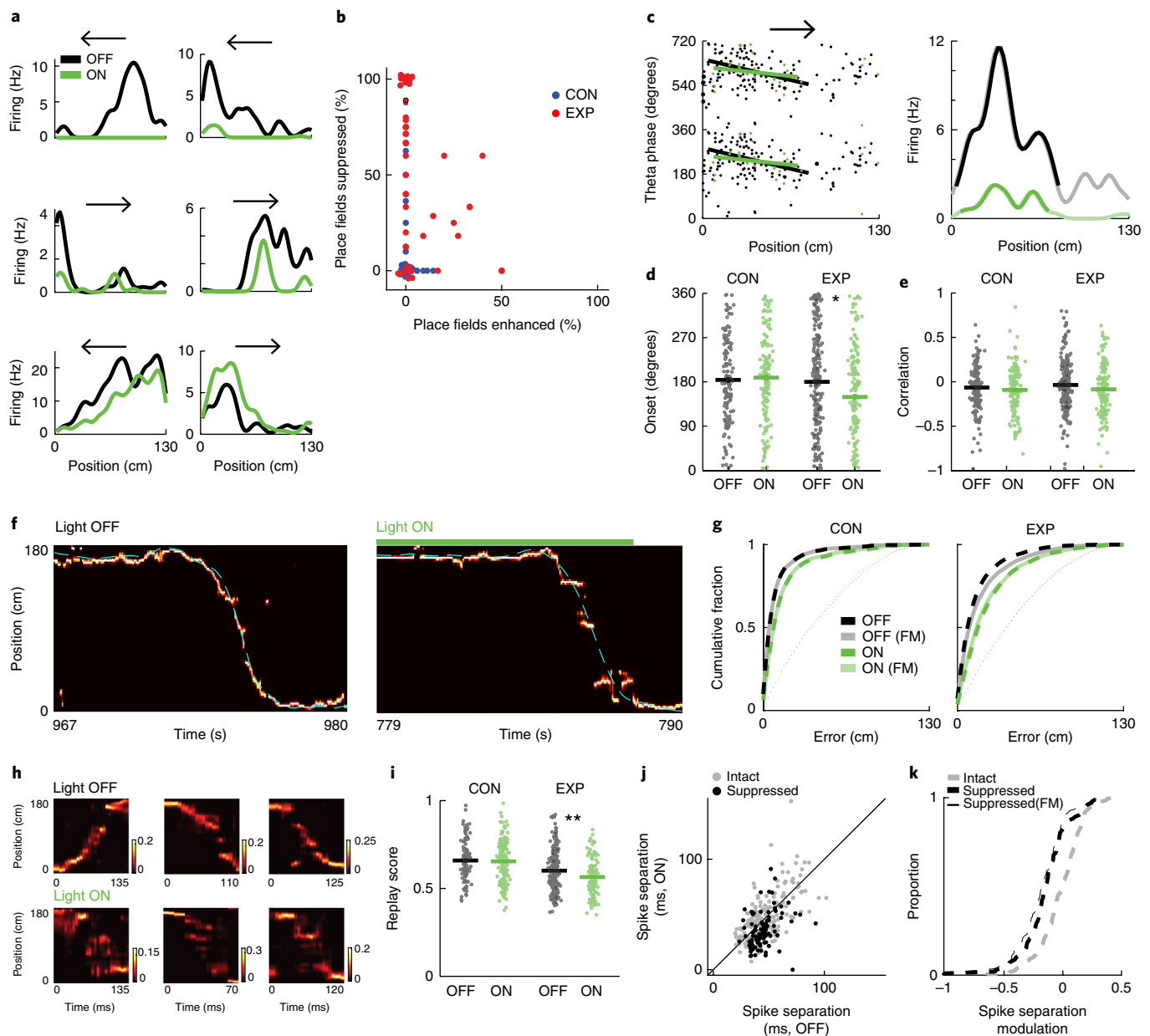


Fig. 3 | Effects of loss of CA3 input on theta precession in CA1 cells and on CA1 ensemble activity. **a**, An example of six place fields simultaneously recorded from a single tetrode in an EXP rat. Arrow depicts running direction. **b**, Heterogeneity in place field responses of each tetrode (dot). For better visualization, noise is added to the corners. Red dot with black circle represents the tetrode in **a**. **c**, An example of phase precession in an EXP place cell. Each dot represents the theta phase of a spike occurring either during light OFF (black) or light ON (green) conditions in relation to rat's position on the track. Regression lines span the field range (left). Right: the corresponding place field in the two light conditions. Transparent color shows the overall firing and dark color shows the field range. **d,e**, Phase precession features presented in mean \pm s.e.m. Precession onset (CON: OFF: $183.99 \pm 6.02^\circ$, Rayleigh test for circular nonuniformity, $n = 135$ fields, $z_{(134)} = 8.8$, $P = 2 \times 10^{-4}$; ON: 188.72 ± 5.93 , Rayleigh test, $n = 144$ fields, $z_{(143)} = 15.8$, $P = 5 \times 10^{-4}$; Watson-Williams test for circular comparison, $n_1 = 135$ and $n_2 = 144$ fields, $F_{(278)} = 0.1$, $P = 0.7$; EXP: OFF: 180.09 ± 5.18 , Rayleigh test, $n = 217$ fields, $z_{(216)} = 2.8$, $P = 0.6$ and ON: $149.34 \pm 6.05^\circ$, Rayleigh test, $n = 142$ fields, $z_{(141)} = 6.2$, $P = 0.002$; Watson-Williams test, $n_1 = 217$ and $n_2 = 142$ fields, $F_{(358)} = 5.0$, $P = 0.025$) (**d**). Precession correlation (CON: two-tailed t test, $n_1 = 135$ and $n_2 = 144$ fields, $F_{(278)} = 0.7$, $P = 0.4$; EXP: two-tailed rank-sum test, $n_1 = 217$ and $n_2 = 142$, $z_{(358)} = 1.7$, $P = 0.10$) (**e**). **f**, Bayesian decoding of rat's position as it traverses the linear track. Population posterior probability (heat plot) is overlaid with rat's actual position (cyan dashed line) in light OFF (left) and light ON (right, green bar) conditions. **g**, CDF of position reconstruction error (CON: two-tailed paired t test, $n = 4$ sessions, $F_{(3)} = 3.4$, $P = 0.16$; EXP: two-tailed paired t test, $n = 8$ sessions, $F_{(7)} = 47.3$, $P = 0.0002$; EXP FM: two-tailed paired t test, $n = 8$ sessions, $F_{(7)} = 36.7$, $P = 0.0005$; EXP OFF versus EXP OFF FM: two-tailed paired t test, $n = 8$ sessions, $F_{(7)} = 7.6$, $P = 0.028$). Dotted lines show the chance level of reconstruction error in two light conditions. **h**, Examples of replays occurring during light OFF (top) and light ON (bottom) conditions in EXP rats. Each panel shows posterior probability of a decoded replay with its corresponding scale bar. **i**, Replay score (CON: two-tailed t test, $n_1 = 99$ and $n_2 = 148$ replays, $F_{(245)} = 0.1$, $P = 0.8$; EXP: two-tailed rank-sum test, $n_1 = 212$ and $n_2 = 121$ replays, $z_{(342)} = 2.6$, $P = 0.0098$). Bars represent mean \pm s.e.m. **j**, In-SWR spike separation in 'intact' and 'suppressed' pairs (intact: OFF: 47.75 ± 1.18 ms (mean \pm s.e.m.) and ON: 48.34 ± 1.75 , two-tailed signed-rank test, $n = 194$ field pairs, $z_{(193)} = 0.2$, $P = 0.8$; suppressed: OFF: 45.09 ± 1.10 and ON: 35.60 ± 1.52 , two-tailed signed-rank test, $n = 102$ field pairs, $z_{(101)} = 5.7$, $P = 2 \times 10^{-8}$). **k**, The CDF of spike separation modulation (intact versus suppressed: two-tailed t test, $n_1 = 194$ and $n_2 = 102$ field pairs, $F_{(294)} = 29.9$, $P = 10^{-7}$; suppressed versus suppressed FM: two-tailed t test, $n_1 = 102$ and $n_2 = 82$, $F_{(182)} = 1.8$, $P = 0.19$). * $P < 0.05$, ** $P < 0.01$.

half of EXP place fields were substantially suppressed (EXP: 49.2%, CON: 3.8%; Fig. 2 and Supplementary Fig. 6). Moreover, 24.1% (28/116) of suppressed EXP fields were completely silenced, in that spiking was abolished. Interestingly, a very few cells enhanced their in-field activity (EXP: 8.1%, CON: 1.9%; Supplementary Fig. 6c) while the remaining cells were unaffected; in some instances possibly due to a lack of impinging light as noted above (EXP: 42.8%, CON: 94.3%). Overall, light caused a major reduction in firing rates in EXP fields, leading to lower in-field peak firing, smaller field size, increased spatial information per spike and less stable yet sharper tuned fields (Fig. 2e–l and Supplementary Fig. 7). Importantly, however, the increase in spatial precision did not reflect an increase in accuracy, rather the reverse was true: measures of the spatial location of the place fields, such as center of mass (COM) and spatial correlation, exhibited significant changes (Fig. 2g,k,l), although skewness was not significantly changed (Supplementary Fig. 7e,f), as changes to this measure are less detectable than for COM¹¹. To examine whether CA3 merely augments spatial information available from other inputs such as cortex, or, alternatively, transmits crucial spatial content unavailable from other inputs, we compared firing-matched place fields in light ON versus light OFF conditions, by downsampling spikes in whichever light condition had the higher total firing rate (Fig. 2i–l). While firing matching resulted in comparable place field peak firing modulation (Fig. 2i), it only partially captured the decrease in place field size (Fig. 2j), lap-by-lap stability (Fig. 2m) and increase in spatial information (Supplementary Fig. 7b) in EXP rats. Moreover, the extent of the deviations in COM (Fig. 2k) and, critically, the decline in spatial correlation (Fig. 2l) in EXP rats were not captured at all by firing matching. These data establish that, for most neurons in the hippocampal output area, the spatial content of CA1 place fields depends heavily on CA3 input, even in a highly familiar environment, and cannot be supported solely by direct cortical input.

We noted that some tetrodes exhibited heterogeneity in the responses of their cells to CA3 suppression (Fig. 3a). Across all tetrodes, the proportion of each tetrode's cells that were excited, unaffected or suppressed varied, with many tetrodes exhibiting 'mixed' populations of cells (Fig. 3b). We examined the locking of activity to hippocampal theta (Supplementary Fig. 8a–d). While the strength of phase locking remained unaffected by light in CON and EXP neurons, the mean phase of locking shifted to earlier phases. Phase precession was not affected by CA3 silencing, including the precession quality, slope and range, consistent with a dependency on direct cortical input¹². However, the onset phase was earlier, matching the mean locking phase (Fig. 3c–e and Supplementary Figs. 8e–g and 9). Together, these results suggest that some cells are less dominated by CA3, and for these, CA3 contributes to the late phase of the theta cycle, consistent with a role in memory retrieval during theta sequences¹³.

We speculated that a further contribution of CA3 might be revealed by examining the coordinated activity of CA1 ensembles. We performed Bayesian decoding of position during traversal of the linear track, revealing that position estimation was degraded in EXP rats in the light ON condition (Fig. 3f,g and Supplementary Fig. 10). The effect was not due to reduced spiking alone, consistent with the spatial correlation changes of individual cells' place fields (Fig. 3g). We further applied our analysis of coordinated activity to address replay during SWRs. Given our finding of a critical role of CA3 in SWRs, we hypothesized that replay would also be affected, and indeed replay quality was degraded in the light ON condition in EXP rats (Fig. 3h,i and Supplementary Fig. 11a). However, a complication for these analyses is the fact that many CA1 cells were not modulated by light condition, probably in part due to variability in light incidence. Therefore, we considered pairwise reactivation, separating pairs of cells both modulated by light during running ('suppressed' pairs) from pairs of cells both non-modulated ('intact' pairs).

First, we examined whether the average time lag ('spike separation') between pairs during SWRs was modulated by light. While spike separation was not affected by light in intact pairs, it was decreased during light ON in suppressed pairs, and this effect was not due to lower spiking during light ON, as verified using the firing rate matching procedure (Fig. 3j,k). As a proxy for replay, it was expected that field pairs with spatially 'close' field peaks would fire temporally close to each other during SWRs, while pairs with spatially 'far' field peaks would fire with a higher spike separation^{14,15}. We found that this pattern held for intact pairs regardless of light condition (Supplementary Fig. 11b); however it was only evident for suppressed pairs in the light OFF condition (Supplementary Fig. 11c). Further, when we applied the firing rate matching procedure to suppressed pairs, the pattern persisted in the light OFF condition, suggesting that spike rates alone could not account for the disruption to replay (Supplementary Fig. 11d). Taken together, these results define CA3 as critical not only for the generation of CA1 SWRs but also for their content.

Several possible caveats were mitigated as follows. Paradoxical increase in spontaneous vesicle release¹⁶ was avoided by using short inactivation periods, and, moreover, we found only minor rebound effects of inhibition. A recent concern for off-target effects is less relevant here since rather than measuring a behavior dependent on the complex interaction of multiple circuits¹⁷, we measured neural activity changes one synapse away. The proximity of area CA2 to the site of adeno-associated virus (AAV) injection was a potential concern, given its direct projection to CA1 and the temporal proximity of its activity to CA1 SWRs⁸. However, CA2 inputs synapse in the CA1 stratum oriens¹⁸, which we avoided as indicated by both electrophysiological and anatomical evidence. The pattern of activity changes observed after suppression of CA3 input was hard to predict a priori, due to diversity in the polarity of projections from ipsilateral and contralateral CA3¹⁹. In summary, we found that a large fraction of individual CA1 neurons were critically dependent on CA3 input, even in a highly familiar environment, while a minority of cells may have been driven more by either cortical or CA2 inputs. Thus, while CA1 activity as a whole may depend on both CA3 and non-CA3 inputs²⁰, CA3 is the predominant driver of CA1 cells under normal conditions.

Online content

Any methods, additional references, Nature Research reporting summaries, source data, statements of data availability and associated accession codes are available at <https://doi.org/10.1038/s41593-018-0321-z>.

Received: 3 July 2018; Accepted: 5 December 2018;

Published online: 21 January 2019

References

- Buzsáki, G. *Hippocampus* **25**, 1073–1188 (2015).
- Mizumori, S. J. Y., McNaughton, B. L., Barnes, C. A. & Fox, K. B. J. *Neurosci.* **9**, 3915–3928 (1989).
- Brun, V. H. et al. *Science* **296**, 2243–2246 (2002).
- Nakashiba, T., Young, J. Z., McHugh, T. J., Buhl, D. L. & Tonegawa, S. *Science* **319**, 1260–1264 (2008).
- Nakashiba, T., Buhl, D. L., McHugh, T. J. & Tonegawa, S. *Neuron* **62**, 781–787 (2009).
- Brun, V. H. et al. *Neuron* **57**, 290–302 (2008).
- Middleton, S. J. & McHugh, T. J. *Nat. Neurosci.* **19**, 945–951 (2016).
- Oliva, A., Fernández-Ruiz, A., Buzsáki, G. & Berényi, A. *Neuron* **91**, 1342–1355 (2016).
- Yamamoto, J. & Tonegawa, S. *Neuron* **96**, 217–227.e4 (2017).
- Keck, T. et al. *Phil. Trans. R. Soc. Lond. B Biol. Sci.* **372**, 20160158 (2017).
- Roth, E. D., Yu, X., Rao, G. & Knierim, J. J. *PLoS One* **7**, e36035 (2012).
- Schlesinger, M. I. et al. *Nat. Neurosci.* **18**, 1123–1132 (2015).
- Feng, T., Silva, D. & Foster, D. J. *J. Neurosci.* **35**, 4890–4902 (2015).
- Suh, J., Foster, D. J., Davoudi, H., Wilson, M. A. & Tonegawa, S. *Neuron* **80**, 484–493 (2013).

15. Karlsson, M. P. & Frank, L. M. *Nat. Neurosci.* **12**, 913–918 (2009).
16. Mahn, M., Prigge, M., Ron, S., Levy, R. & Yizhar, O. *Nat. Neurosci.* **19**, 554–556 (2016).
17. Otchy, T. M. et al. *Nature* **528**, 358–363 (2015).
18. Dudek, S. M., Alexander, G. M. & Farris, S. *Nat. Rev. Neurosci.* **17**, 89–102 (2016).
19. Zugaro, M. B., Monconduit, L. & Buzsáki, G. *Nat. Neurosci.* **8**, 67–71 (2005).
20. Ahmed, O. J. & Mehta, M. R. *Trends Neurosci.* **32**, 329–338 (2009).

Acknowledgements

This work was supported by The McKnight Endowment Fund for Neuroscience (D.J.F.) and National Institute of Mental Health grant R01 MH103325 (D.J.F.). We thank Zeinab Vessal for graphic design. For imaging facility, we thank M. Pucak at Multiphoton Imaging Core (center grant: P30 NINDS 050274) at Department of Neuroscience, Johns Hopkins University and H. Aaron and F. Ives at CRL Molecular Imaging Center (Biological Research Faculty Grant) at UC Berkeley.

Author contributions

H.D. and D.J.F. conceived the project, designed the experiments, and wrote the paper. H.D. performed the experiments and collected and analyzed the data.

Competing interests

The authors declare no competing interests.

Additional information

Supplementary information is available for this paper at <https://doi.org/10.1038/s41593-018-0321-z>.

Reprints and permissions information is available at www.nature.com/reprints.

Correspondence and requests for materials should be addressed to D.J.F.

Publisher's note: Springer Nature remains neutral with regard to jurisdictional claims in published maps and institutional affiliations.

© The Author(s), under exclusive licence to Springer Nature America, Inc. 2019

Methods

Animal training. A total of six adult male Long-Evans rats (2–3 months old, 250–400 g) were used for this study. All procedures were approved by Johns Hopkins University Animal Care and Use Committee and followed US National Institutes of Health animal use guidelines. Animals were housed on a standard, non-inverted, 12-h light cycle. Rats were food-restricted to achieve ~90% of their normal weight and then trained to traverse a 165-cm linear track to receive a liquid chocolate-flavored reward (200 μ l, Carnation) at wells in either side of the track. Rats were trained for 30–40 complete laps once per day for 5–7 consecutive days on a familiar track. With this ~200 traversals, rats became highly familiar with the task, the track and the environment.

Optogenetics setup. Each trained rat underwent two surgeries. The first surgery was for injecting AAV-containing light-sensitive protein Archaelhodopsin (eArch3.0) to CA3. At least four weeks after injection, when CA3 cell bodies and axons strongly expressed eArch3.0 gene, the optetrode drive was implanted. The details of each of these steps are as follows.

Virus transduction (first surgery). We chose AAV5 due to its transduction efficiency and high expression level of proton pump eArch3.0 in conjunction with a CamKII α promoter that specifically targets pyramidal cells and not interneurons^{21,22}. All viral constructs were provided from University of North Carolina Vector Core under material transfer agreement with Karl Deisseroth laboratory.

Four experimental (EXP) rats were injected with AAV5_CamKII α _eArch3.0_EYFP and two control (CON) rats were injected with AAV5_CamKII α _EYFP in each of six sites in their dorsal and intermediate CA3a and b. A total of 6 μ l of virus (1 μ l in each site) were stereotaxically injected in each rat (AP = -3.1 mm, ML = \pm 3.5 and DV = -3.5), (AP = -4.0 mm, ML = \pm 4.3 and DV = -4) and (AP = -4.7 mm, ML = \pm 4.8, and DV = -4.8) where AP, ML and DV stand for anterior-posterior in relation to bregma, medio-lateral and dorso-ventral axes in relation to surface of skull, respectively.

Optetrode design and implantation (second surgery). A bilateral optetrode with two optical fibers (200 μ m diameter) and up to 40 tetrodes (20 tetrodes in each hemisphere) was designed. For monitoring the position of each optical fiber in the brain, a 'piggy-back' tetrode was glued to and flush with the bottom of each optical fiber. Fibers and all tetrodes were independently adjustable. Each tetrode consisted of a twisted bundle of four 17.8 μ m platinum/10% iridium wires (Neuralynx), and by gold-plating the tip of each tetrode an impedance of <150 k Ω was achieved before implantation.

At least four weeks after viral injection, optetrodes were implanted on rats. Following surgical implantation, optical fibers and tetrodes were slowly lowered into the dorsal CA1 pyramidal layer over a few days using characteristic LFP patterns (mostly SWRs) and spiking patterns as a guide. Placement of tetrodes and recordings were performed as previously described²³. Optical fibers were adjusted to stay in stratum pyramidale, to be able to silence the stratum radiatum in dorsal CA1.

Immunohistochemistry and imaging. For localizing example tetrodes, five tetrodes in each hemisphere received electric lesion (20 μ A DC current for 4 s) before perfusing a rat. Collected brains were fixed by 4% paraformaldehyde in 0.1 M sodium phosphate buffer (PBS), and preserved in 30% sucrose dissolved in PBS. Slices 60 μ m thick were prepared by cryostat and were mounted on slides. For defining CA2 region (PCP4 labeling), slices were first rinsed by 3 \times 10 min PBS and were blocked for 2 h by blocking buffer (3% normal donkey serum with 0.3% Triton-X in PBS). Then, slices were kept overnight in blocking buffer containing primary antibody (Rabbit α -PCP4, 1:500, Proteintech, catalog no. 14705-1-AP). After 3 \times 10 min PBS wash they were kept in blocking buffer containing secondary antibody (Alexa Fluor 594-conjugated donkey α -rabbit, 1:200, Invitrogen A21207). These antibodies have been validated in previous literature²⁴. For background staining of the whole brain, after 3 \times 10 min PBS wash, Hoechst 33258 (1:2,000) in PBS was applied to slices for 10 min and after 3 \times 10 min PBS wash slices were covered with mounting media (Vectashield, Vector Laboratories Inc.) and coverslip. Therefore, whole brain (blue signal via Hoechst 33258), CA3 cell bodies and axons (green signal via AAV-injected EYFP expression with no signal enhancement) and CA2 region (red signal, via PCP4 labeling) were imaged.

Imaging was performed in Multiphoton Imaging Core at Department of Neuroscience, Johns Hopkins University and CRL Molecular Imaging Center at UC Berkeley. For tiled epifluorescence imaging of the whole brain and whole hippocampal area CA3 we used Zeiss Cell Observer and Zeiss AxioScan Z.1 systems. For high-resolution imaging of zoomed areas in CA3 and CA1 a Zeiss LSM 510 confocal imaging system was used.

LFP and cellular unit recording. All data were collected using Digital Lynx data acquisition system (Neuralynx). The rat's position was tracked in darkness via blue and red LEDs mounted on the optetrode, and continuously recorded at 30 frames per second by an overhead camera. Analog neural signals were digitized at 32,000 Hz. The threshold for spike (extracellular action potential) detection was set to 50 μ V. LFP data were digitally filtered between 0.1 and 500 Hz and recorded at 3,200 Hz after ten times downsampling. Individual units were also identified by

manual clustering on the basis of spike waveform peak amplitudes using a custom software (xclust2, M. A. Wilson, MIT).

Task design. A recording day consisted of a one-hour recording session in a sleep box ('Pre' rest session), followed by 20–35 traversing laps (lasting ~15–30 min) on a familiar 165 cm linear track ('Run' session), and one hour of recording in the sleep box ('Post' rest session). One limitation of optogenetic silencing using eArch3.0 is that minutes-long-sustained illumination may paradoxically result in increased spontaneous vesicle release in axon terminals¹⁶. However, we avoided this issue by limiting our experimental design to shorter (<1 min) inactivation of CA3 axons. In each rest session, light was delivered in four pulse trains, each lasting 400 s. Each pulse train consisted of alternating 20-s light on stimulation periods followed by 20-s light off periods, with this on/off cycle repeating 10 times. Light was delivered from a 532 nm (green) laser and the estimated light power at the tips of optical fibers in each hemisphere was around 3.25 mW (light power density: 100 mW mm⁻²). Laser commands were generated by a custom-written MATLAB (Mathworks) graphic user interface and were delivered to laser by multifunction data acquisition device NI USB-6341 (National Instruments).

Next, rats were put on a highly familiar linear track. For the Run session, light was manually and consecutively turned on and off for light ON and light OFF laps. For each light ON lap, light was continuously on while the rat was traversing the track, staying at one end of the track and returning to the first position. For each rat, in different sessions, we usually switched the light stimulation pattern on track to remove the bias of the animal to one end of the track in the recording room. The stimulation pattern for 'Post' rest sessions were similar to 'Pre' rest sessions.

LFP analysis. All tetrodes that were able to detect SWRs (with incidence rate of more than 0.05 SWR s⁻¹ in either light OFF or light ON conditions) were included in the LFP analysis, regardless of whether they showed any modulation by light or not. For SWR detection in the sleep box, only 'Pre' rest sessions were analyzed and, using a speed threshold of 7 cm s⁻¹, moments that rat intensely moved were excluded from the analysis. One electrode from each acceptable tetrode was considered for LFP analysis. To avoid repetitive measurements, for each tetrode only the session in which it had a maximum baseline (5–10 min pre-stimulus recording) SWR incidence rate was selected. The LFP signal of each electrode was denoised for 60 Hz electric noise and its 180 Hz harmonic using a second-order IIR notch filter. Then, denoised LFP was filtered at SWR frequency range (100–250 Hz) with a fifth-order Butterworth band-pass filter. The envelopes of each band-passed LFP were obtained using the absolute value of its Hilbert transform. After applying a Gaussian smoothing filter with 5 ms standard deviation, the envelope was z scored. Events that passed five standard deviations (that is, mean + 5 s.d. of averaged non-z scored envelope) were considered as candidate SWR events, and SWRs that were less than 10 ms apart were merged and considered as one extended ripple. The beginning and end of each SWR were defined as where the smoothed envelope crossed its one standard deviation value, and events lasting less than 20 ms were removed. Tetrodes with SWR incidence rate of more than 0.05 SWR s⁻¹ (for example at least one ripple event on average in every 20 s either during light OFF or light ON periods) were considered for further analysis.

Place field analysis. Place field calculation and features. Due to manual commanding of laser, there was a variability in the start time of light ON laps. Therefore, the reward zones on either side of the track (17.5 cm each side) were excluded and only the middle 130 cm of the 165-cm-long track was considered for place field calculation. All the place cell analyses, except spatial coherence, were done on one-dimensional place fields. One-dimensional place fields were obtained by binning the linear track using 2 cm bins, and the raw place field was smoothed by applying a Gaussian filter with a 5 cm standard deviation. Also, all analyses were done independently on directional fields in light OFF and light ON conditions. To avoid repetitive inclusion of place cells from different sessions, for each tetrode only the session in which it had most place cells was considered for analysis. To have a relatively inclusive definition, only cells that met all the following criteria either in light OFF or light ON conditions were considered as place cells. These consist of a peak field firing rate >1 Hz, spatial coherence >0.1, lap-by-lap stability >0.2 and number of spiking laps >5. Moreover, place fields that covered the whole track with a low spatial information (<0.15) were considered as truncated place fields and were omitted.

Place field features were calculated as follows. Place field size was calculated as the number of contiguous 2-cm-wide bins above 20% of peak place field firing. For features such as peak firing rate and field size, all place fields from light OFF and light ON conditions were included in the analysis (as far as the field passed the aforementioned criteria at least in one light condition). For example, if a place field gets completely suppressed in light ON condition, its peak firing rate and field size become zero and are included in the analysis. However, for the following features, only fields that passed the criteria in at least one light condition and had at least one spike in the other condition were included in the analysis.

The sparsity index ranges from 0 to 1, where a lower value means a less diffuse and more spatially specific place field²⁵. Sparsity is defined as:

$$\text{Sparsity} = \frac{\left(\sum_{i=1}^n p_i f_i\right)^2}{\sum_{i=1}^n p_i f_i^2}$$

where each 2 cm bin ($n = 65$) has firing rate f_i and occupancy time t_i , and p_i is the occupancy probability: $p_i = t_i / \sum_{i=1}^n t_i$

Spatial information, which is the amount of information about an animal's position conveyed by each spike, is calculated as follows²⁵:

$$\text{Spatial information} = \sum_{i=1}^n p_i \frac{f_i}{f} \log_2 \frac{f_i}{f}$$

where f is the mean firing rate, $f = \sum_{i=1}^n p_i f_i$.

The center of mass (COM) of a place field was calculated using the following equation:

$$\text{COM} = \frac{\sum_{i=1}^n x_i f_i}{\sum_{i=1}^n f_i}$$

where x_i is the i th position bin on the track.

The skewness of each place field was defined as:

$$\text{Skewness} = \frac{\sum_{i=1}^n f_i (x_i - \text{mean}(x))^3}{\sigma_x^{3/2} \sum_{i=1}^n f_i}$$

with σ_x defined as:

$$\sigma_x = \frac{\sum_{i=1}^n f_i (x_i - \text{mean}(x))^2}{\sum_{i=1}^n f_i}$$

Spatial coherence, which quantifies smoothness and local orderliness of a place field, is the autocorrelation of each place field with its nearest neighbor average²⁶. To do this, the $6 \times 130 \text{ cm}^2$ linear track was binned into $2 \times 2 \text{ cm}^2$ bins and the new firing map for each pixel was calculated as the average firing rate of the eight unsmoothed neighbor pixels. Then, the two-dimensional correlation coefficient between the original unsmoothed firing map and the new one was calculated and, to be statistically comparable, we applied a Fisher transform (or z transform, $z = \text{arctanh}(r)$) on correlation coefficients before calculating z values.

Lap-by-lap stability was defined as the average of the correlation of the place field for each spiking lap with the overall place field. This measure was separately calculated for light OFF and light ON laps.

Spatial correlation, which was defined as the normalized Pearson correlation coefficient of place fields in light OFF and light ON conditions, was also Fisher-transformed for statistical comparison.

The modulation effect significance was calculated for each place field by comparing its lap-by-lap spike counts per second in light OFF versus light ON laps. For each tetrad a two-dimensional heterogeneity value was defined as the percentage of its fields that were statistically significantly suppressed versus the percentage of its fields that were statistically significantly enhanced.

Place cell firing matching. To test whether the partial suppression of CA3 input simply downsamples the number of CA1 place cell spikes, or CA1 spatial coding is more systematically disrupted, the total firing rate of each place field was matched in light OFF and light ON conditions. For each corresponding OFF and ON fields, the spikes of whichever field with higher total firing rate were randomly omitted to the extent of reaching a matched total firing rate. Then, all place field features were calculated for the firing-matched OFF and ON fields, separately for CON and EXP rats.

Theta analysis. Theta phase locking. For the temporal coding analysis, only place fields that not only passed the aforementioned criteria but also contained at least ten in-field spikes in both light OFF and light ON conditions were considered for further theta phase locking and phase precession analysis. We chose these relatively low criteria to be more inclusive in studying the effect of field suppression on its temporal coding properties.

For each tetrad, the instantaneous theta phase was calculated using the Hilbert transform of theta-band-filtered LFP. For each session, we chose a tetrad with high theta power as global reference theta. Then, for each place cell, spikes and LFP time stamps were used to linearly interpolate theta phase for each spike. The degree of modulation of each place cell by theta phase was obtained by calculating its circular mean resultant vector (MRV). MRV may vary from 0 (no phase preference) to 1 (every spike occurred at the same theta phase). To make recording sessions comparable, by using multi-unit activity of all the clustered cells, global reference theta was shifted in a way that maximum multi-unit firing occurs at the trough (180°) of theta rhythm.

Theta phase precession. To calculate theta phase precession²⁵, circular-linear regression was used²⁷. A linear model $\varphi(x) = 2\pi ax + \varphi_0$ was fit into phase-position circular-linear pairs $\{x_i, \varphi_i\}_n$ for each place cell independently for ON and OFF place fields. The precession slope a was varied in the range $\mathcal{C} = (-10, 10)$, which is equivalent to $(-27.69^\circ \text{ cm}^{-1}, 27.69^\circ \text{ cm}^{-1})$, to find the optimal $\hat{a} = \text{argmax}_{a \in \mathcal{C}} R(a)$

that maximizes $R(a)$, the MRV of the circular errors between the measured phase φ_i and the model predictions $\varphi(x)$:

$$R(a) = \frac{1}{\sqrt{\left(\frac{1}{n} \sum_{i=1}^n \cos(\varphi_i - 2\pi ax_i) \right)^2 + \left(\frac{1}{n} \sum_{i=1}^n \sin(\varphi_i - 2\pi ax_i) \right)^2}}$$

Next, the phase offset $\hat{\varphi}_0$ is calculated as follows:

$$\hat{\varphi}_0 = \arctan 2 \frac{\sum_{i=1}^n \sin(\varphi_i - 2\pi \hat{a} x_i)}{\sum_{i=1}^n \cos(\varphi_i - 2\pi \hat{a} x_i)}$$

Then, the circular-linear correlation coefficient is calculated as follows:

$$\rho = \frac{\sum_{i=1}^n \sin(\varphi_i - \bar{\varphi}) \sin(\theta_i - \bar{\theta})}{\sqrt{\sum_{i=1}^n \sin(\varphi_i - \bar{\varphi})^2 \sum_{i=1}^n \sin(\theta_i - \bar{\theta})^2}}$$

where $\bar{\varphi} = \frac{\sum_{i=1}^n \sin(\varphi_i)}{\sum_{i=1}^n \cos(\varphi_i)}$ and $\bar{\theta} = \frac{\sum_{i=1}^n \sin(\theta_i)}{\sum_{i=1}^n \cos(\theta_i)}$, and $\theta_i = 2\pi \hat{a} |x_i \pmod{2\pi}$ is the linearly fitted phase. To determine statistical significance, the scaled correlation is calculated. For large n and under the null hypothesis that phases are from an uncorrelated Gaussian random distribution, the scaled correlation is given by

$$z = \rho \sqrt{\frac{\lambda_{02} \lambda_{20}}{\lambda_{22}}}$$

where

$$\lambda_{ij} = \frac{1}{n} \sum_{k=1}^n \sin^i(\varphi_k - \bar{\varphi}) \sin^j(\theta_k - \bar{\theta})$$

Given z , the significance value can be derived from the cumulative normal distribution:

$$p = 1 - \text{erf}\left(\frac{|z|}{\sqrt{2}}\right)$$

Once the linear regression parameters were calculated, precession phase onset and range were respectively derived by the multiplication of the beginning and the size of a place field by the precession slope.

Neural population analysis. Bayesian decoding of position. A Bayesian probability-based decoding algorithm for estimating animal's position was performed²⁸. The posterior probability (Prob) of the animal's position (P) in each running direction (dir) across N_p total position bins given a time window containing neural spiking (spikes) from N_r directional place fields is

$$\text{rob}_{dir}(P | \text{spikes}) = U_{dir} / \sum_{j=1}^{N_p} U_{dir}$$

where

$$U_{dir} = \prod_{i=1}^{N_r} f_i(P, dir)^{n_i} \exp\left(-i \sum_{i=1}^{N_r} f_i(P, dir)\right)$$

and $f_i(P, dir)$ is the i th place field in a running direction, assuming independent rates and Poisson firing statistics for all N fields and a uniform prior over position. n_i is the number of spikes in i th place field in a time window of 400 ms which was used to estimate the rat's position on a behavioral timescale. This time window was slid by 50 ms timesteps. OFF fields were used for decoding position during both light OFF and light ON conditions because ON fields were highly suppressed, resulting in an even more degraded decoding. Also, since rats did head-sweeping beyond the ends of track we considered a 180 cm position range (15 cm extension to 165 cm track) for better decoding of behavior at the ends of track. For this purpose, we recalculated place fields and included cells that fired at the ends of tracks. This was only for visualization purposes and for run decoding error analysis we stayed with the original 130-cm-range place fields.

Position reconstruction error during Run was defined as the average distance between the animal's current location and the peak decoded position in each 200-ms time bin while the rat was traversing the track with a $>7 \text{ cm s}^{-1}$ speed. Chance level of reconstruction error was determined by performing the same calculation except substituting the peak decoded positions with random positions. To test whether the degradation in positional decoding is merely due to lower spiking of place cells under light, we performed firing matching of individual place cells as described in the section 'Place cell firing matching' and then recalculated the position reconstruction error.

Replay decoding and characterization. Each global SWR event (detected from average z -scored LFP of all tetrodes) was considered as a candidate population event in which a time window of 20 ms sliding in 5-ms steps was used to estimate position. Because replays start at the ends of track where rats are at rest or head-sweeping we considered a 180 cm position range for Bayesian decoding of replays. To calculate the statistical significance of each candidate event with two-dimensional weighted correlation more than 0.5, place field identities were randomly shuffled for 1,000 times and P value was calculated by the Monte Carlo method: $P = (n + 1)/(s + 1)$, where s is the total number of shuffled datasets and n is the number of shuffled datasets that produced a number of correlated events greater than or equal to the correlation of candidate event. Candidate events with $P < 0.05$ were considered as replays. Replays were characterized with two measures, that is replay score and replay speed. They were defined as where the likelihood (R) that a replay is along the fitted line with slope v and starting location ρ is maximized²⁸. R was calculated as the averaged decoded probability in a vicinity (vic) along the fitted line:

$$R(v, \rho) = \frac{1}{N_T} \sum_{i=0}^{N_T-1} \sum_{j \in vic} Prob_{ij}(|P - (\rho + v \cdot i \cdot \Delta t)| \leq d)$$

where Δt is the moving step of the decoding time window (5 ms) and the value of d was empirically set to 15 cm for capturing local variations in slope. If for a time bin i the fitted line would specify a location beyond the ends of the track, the median probability of all possible locations was taken as the likelihood. To determine the most likely slope for each replay, we densely sampled the parameter space of v and ρ to find the values v_{max} and ρ_{max} that together maximize R . Replay speed is defined as $|v_{max}|$ in $m s^{-1}$ and replay slope is the value of R_{max} .

Pairwise reactivation analysis. To measure the degree to which cells fire with a certain time lag during SWRs, we took spike counts in consecutive 5-ms time bins during and in the vicinity (50 ms of each side) of SWRs, separately for light OFF and light ON conditions. Average time lag or 'spike separation' of each pair was defined as the center of mass of absolute value of the cross-correlation coefficient of two spike count trains (50 bins = 250 ms sweeping in each temporal direction). Therefore, for each cell pair spike the separation measure was calculated separately for light OFF and light ON conditions. Correspondingly, spike separation modulation was defined as $(ON - OFF)/(ON + OFF)$. To refine the effect of light on cell pairs we separated 'suppressed' pairs, that is cell pairs where their associated place fields were both suppressed by light from 'intact' pairs, which are cell pairs where their fields were unaffected by light. Cell pairs with complete suppression of either of their associated place fields during light OFF condition were excluded from the analysis. Moreover, any pair where either of its two spike count trains had less than 20 bins with non-zero value during light OFF condition was excluded from analysis. To investigate whether the observed effects were due to less spiking during light ON condition we did a firing matching for in-SWR spike count trains. Spike downsampling for each spike count train was only applied to whichever light condition had the higher in-SWR firing rate. The amount of downsampling was proportional to the ratio of in-SWR firing rate in the two light conditions. After averaging the 20-times random firing matching of spike count trains, the spike separations for all 'suppressed' pairs were calculated. Existence of replays predicts that field pairs with 'close' field peaks will fire with a lower spike separation than

pairs with 'far' peaks. A threshold distance of 65 cm (that is half of the 130-cm running part of the track) was selected to define close versus far pairs. Distances between OFF fields were used for applying this threshold for both light OFF and light ON conditions. Consequently, spike separations were separately calculated for intact, suppressed and firing-matched pairs during light OFF and light ON conditions.

Statistical analysis and reproducibility. No statistical methods were used to predetermine sample sizes but our sample sizes are similar to those reported in previous publications²⁹. Animals were randomly selected to be in either the CON or EXP groups by being injected either with GFP or eArch3.0, respectively. Data collection and analysis were not performed blind to the conditions of the experiments.

For most analyses, if data points had a Gaussian distribution (checked by Lilliefors test), depending on the type of comparison a two-tailed paired-sample or two-sample t -test was applied. For non-Gaussian distributions, depending on the type of comparison, the non-parametric two-tailed paired-sample Wilcoxon signed rank test or two-tailed two-sample Wilcoxon rank-sum test (also known as the Mann-Whitney U test) was used. The modulation index for each place field feature was defined as $(ON - OFF)/(ON + OFF)$. For example, for place field peak modulation, a modulation index of -1 means complete suppression, 0 means no modulation and a positive value means an enhancement in peak firing. For COM, this index was simply defined as $(ON - OFF)/130$. For circular statistics the CircStat Matlab toolbox was used³⁰. Circular Rayleigh test and Watson-Williams test were used, respectively, to test for non-uniformity and for comparison of two population phases.

Reporting Summary. Further information on research design is available in the Nature Research Reporting Summary linked to this article.

Code availability. The code that support the findings of this study are available from the corresponding author upon reasonable request.

Data availability

The data that support the findings of this study are available from the corresponding author upon reasonable request.

References

1. Yizhar, O., Fenno, L. E., Davidson, T. J., Mogri, M. & Deisseroth, K. *Neuron* **71**, 9–34 (2011).
2. Gradinaru, V. et al. *Cell* **141**, 154–165 (2010).
3. Foster, D. J. & Wilson, M. A. *Nature* **440**, 680–683 (2006).
4. Boehringer, R. et al. *Neuron* **94**, 642–655 (2017).
5. Skaggs, W. E., McNaughton, B. L., Wilson, M. A. & Barnes, C. A. *Hippocampus* **6**, 149–172 (1996).
6. Muller, R. U. & Kubie, J. L. *J. Neurosci.* **9**, 4101–4110 (1989).
7. Kempter, R., Leibold, C., Buzsáki, G., Diba, K. & Schmidt, R. *J. Neurosci. Methods* **207**, 113–124 (2012).
8. Davidson, T. J., Kloosterman, F. & Wilson, M. A. *Neuron* **63**, 497–507 (2009).
9. Rueckemann, J. W. et al. *Hippocampus* **26**, 246–260 (2016).
10. Berens, P. *J. Stat. Softw.* **31**, i10 (2009).

Reporting Summary

Nature Research wishes to improve the reproducibility of the work that we publish. This form provides structure for consistency and transparency in reporting. For further information on Nature Research policies, see [Authors & Referees](#) and the [Editorial Policy Checklist](#).

Statistical parameters

When statistical analyses are reported, confirm that the following items are present in the relevant location (e.g. figure legend, table legend, main text, or Methods section).

n/a Confirmed

- The exact sample size (n) for each experimental group/condition, given as a discrete number and unit of measurement
- An indication of whether measurements were taken from distinct samples or whether the same sample was measured repeatedly
- The statistical test(s) used AND whether they are one- or two-sided
Only common tests should be described solely by name; describe more complex techniques in the Methods section.
- A description of all covariates tested
- A description of any assumptions or corrections, such as tests of normality and adjustment for multiple comparisons
- A full description of the statistics including central tendency (e.g. means) or other basic estimates (e.g. regression coefficient) AND variation (e.g. standard deviation) or associated estimates of uncertainty (e.g. confidence intervals)
- For null hypothesis testing, the test statistic (e.g. F , t , r) with confidence intervals, effect sizes, degrees of freedom and P value noted
Give P values as exact values whenever suitable.
- For Bayesian analysis, information on the choice of priors and Markov chain Monte Carlo settings
- For hierarchical and complex designs, identification of the appropriate level for tests and full reporting of outcomes
- Estimates of effect sizes (e.g. Cohen's d , Pearson's r), indicating how they were calculated
- Clearly defined error bars
State explicitly what error bars represent (e.g. SD, SE, CI)

Our web collection on [statistics for biologists](#) may be useful.

Software and code

Policy information about [availability of computer code](#)

Data collection	Electrophysiological data were collected using Neuralynx software.
Data analysis	Custom codes written in Matlab (MathWorks, Inc) were used to analyze all data. Cell clustering was performed by custom "xclust2" software.

For manuscripts utilizing custom algorithms or software that are central to the research but not yet described in published literature, software must be made available to editors/reviewers upon request. We strongly encourage code deposition in a community repository (e.g. GitHub). See the Nature Research [guidelines for submitting code & software](#) for further information.

Data

Policy information about [availability of data](#)

All manuscripts must include a [data availability statement](#). This statement should provide the following information, where applicable:

- Accession codes, unique identifiers, or web links for publicly available datasets
- A list of figures that have associated raw data
- A description of any restrictions on data availability

The data that support the findings of this study are available from the corresponding author upon reasonable request.

Field-specific reporting

Please select the best fit for your research. If you are not sure, read the appropriate sections before making your selection.

Life sciences Behavioural & social sciences Ecological, evolutionary & environmental sciences

For a reference copy of the document with all sections, see [nature.com/authors/policies/ReportingSummary-flat.pdf](https://www.nature.com/authors/policies/ReportingSummary-flat.pdf)

Life sciences study design

All studies must disclose on these points even when the disclosure is negative.

Sample size	No statistical method were used to predetermined sample size. However, our sample sizes are similar to those reported in previous literature. We used four experimental (EXP) and two control (CON) rats. Since this is an optogenetics study each EXP rat also has its own control condition when laser light is off. This number of animals are comparable with previous optogenetics studies as well.
Data exclusions	Tetrodes that detected SWRs with incidence rate of < 0.05 SWR/s in both light OFF and light ON conditions were excluded from the LFP analysis.
Replication	All four EXP rats, show a significant suppression of sharp-wave ripple incidence rate both in the sleep box session and the linear track session. Moreover, rest-state spiking activity activity was significantly suppressed for all except one rat. These are clearly described in Supplementary Figures.
Randomization	Animals were randomly selected to be in either the CON or EXP groups by being injected either with GFP or eArch3.0, respectively.
Blinding	Data collection and analysis were not performed blind to the conditions of the experiments. For analysis, the exact same code ran for EXP and CON rats.

Reporting for specific materials, systems and methods

Materials & experimental systems

n/a	Involvement in the study
<input type="checkbox"/>	<input checked="" type="checkbox"/> Unique biological materials
<input type="checkbox"/>	<input checked="" type="checkbox"/> Antibodies
<input checked="" type="checkbox"/>	<input type="checkbox"/> Eukaryotic cell lines
<input checked="" type="checkbox"/>	<input type="checkbox"/> Palaeontology
<input type="checkbox"/>	<input checked="" type="checkbox"/> Animals and other organisms
<input checked="" type="checkbox"/>	<input type="checkbox"/> Human research participants

Methods

n/a	Involvement in the study
<input checked="" type="checkbox"/>	<input type="checkbox"/> ChIP-seq
<input checked="" type="checkbox"/>	<input type="checkbox"/> Flow cytometry
<input checked="" type="checkbox"/>	<input type="checkbox"/> MRI-based neuroimaging

Unique biological materials

Policy information about [availability of materials](#)

Obtaining unique materials	No for-profit material is produced in this paper. All viral constructs were provided from University of North Carolina Vector Core under material transfer agreement with Karl Deisseroth laboratory. As mentioned in the Data and Code Availability sections of the Supplementary Methods, all data and code are available to public upon reasonable request.
----------------------------	--

Antibodies

Antibodies used	Primary antibody: Rabbit α -PCP4, Proteintech, Cat# 14705-1-AP, dilution: 1:500. Secondary antibody: Alexa Fluor 594-conjugated donkey α -rabbit, Invitrogen, Cat# A21207, dilution: 1:200.
Validation	These antibodies have been validated in previous literature (ref. 4: Boehringer et al, 2017).

Animals and other organisms

Policy information about [studies involving animals](#); [ARRIVE guidelines](#) recommended for reporting animal research

Laboratory animals

A total of six Adult male Long-Evans rats (2-3 months old, 250-400 g) were used for this study. It is described in Supplementary Methods.

Wild animals

No wild animals were used in this study.

Field-collected samples

No field-collected samples were used in this study.